

# Finite element inspired networks: Learning physically-plausible deformable object dynamics from partial observations

Shamil Mamedov<sup>\*,1</sup> A. René Geist<sup>\*,2</sup> Jan Swevers<sup>1</sup> Sebastian Trimpe<sup>2</sup>

<sup>1</sup>MECO Research Team, KU Leuven

<sup>2</sup>Institute for Data Science in Mechanical Engineering, RWTH Aachen University

**Abstract:** The accurate simulation of deformable linear object (DLO) dynamics is challenging if the task at hand requires a human-interpretable and data-efficient model that also yields fast predictions. To arrive at such model, we draw inspiration from the rigid finite element method (R-FEM) and model a DLO as a serial chain of rigid bodies whose internal state is unrolled through time by a dynamics network. As this state is not observed directly, the dynamics network is trained jointly with a physics-informed encoder mapping observed motion variables to the body chain’s state. To encourage that the state acquires a physically meaningful representation, we leverage the forward kinematics (FK) of the underlying R-FEM model as a decoder. We demonstrate in a robot experiment that this architecture – being termed “Finite element inspired network” – forms an easy to handle, yet capable DLO dynamics model yielding physically interpretable predictions from partial observations.

The project code is available at: <https://tinyurl.com/fei-networks>

**Keywords:** Physics-inspired machine learning, Rigid finite element method

## 1 Introduction

Deformable linear objects (DLOs) (e.g., cables, ropes, and threads) are prevalent in various promising applications within the field of robotics [1, 2]. Dynamics models empower robots to interact with DLO, showcasing remarkable dexterity at tasks such as intricate knotting [3, 4], precise manipulation of ropes [5], and surgical suturing [6, 7]. Furthermore, the parts of many robots can be modeled as DLO themselves. This naturally applies to numerous soft robots but is also relevant for the control of supposedly rigid industrial robots. For example, the significant end-effector forces arising in robot machining cause elastic deformations which if not being modeled accurately, reduce manufacturing precision [8, 9]. In addition, designing manipulators and legged robots to be lightweight yet flexible, potentially lowers the robot’s manufacturing costs, increases its maximum attainable joint accelerations, and benefits its energy efficiency [10].

Yet, the acquisition of accurate DLO dynamics models forms still a significant challenge [1, 2]. In this regard, the identification of DLO dynamics via purely data-driven models, such as neural networks (NNs), is hindered by several practical issues. Firstly, on robotic systems data is collected in real-time, substantially raising the cost of collecting large data sets. Thereby, data sets collected on robots are relatively small which hinders the usage of large NNs. Moreover, the information contained within the data is significantly affected by the input excitation signal used for data collection. This raises the question of how to design dynamics models that generalize from training data to unseen points in the system’s state space. Secondly, it is not clear what constitutes the state of a DLO

---

<sup>\*</sup>Equal contribution.

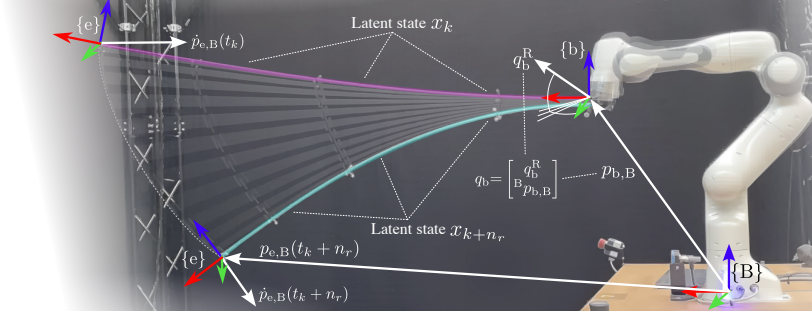


Figure 1: A DLO is actuated by a robot arm. Given observations of  $\{b\}$  and  $\{e\}$  (only first time step), a FEI network predicts the motion of  $\{e\}$ 's origin while also estimating the DLO's shape.

and what observations are required to identify its dynamics. To surmount the inherent challenges that underlie learning DLO dynamics, we draw inspiration from multibody mechanics and view a DLO as a chain of rigid bodies that are connected through joint forces. Through this perspective, we arrive at finite-element inspired (FEI) networks.

### 1.1 Overview and Contributions

Figure 1 provides an overview of the experimental setup and notation used. In what follows,  $x \in \mathbb{R}^{n_x}$  denotes the unobserved state of the body chain,  $\{B\}$  denotes an inertial coordinate frame (aka frame),  $\{b\}$  denotes a frame being fixed to the DLO's start, and  $\{e\}$  denotes a frame being fixed to the DLO's end. At the initial prediction time, the pose of  $\{b\}$  and  $\{e\}$  is observed yielding  $h = ({}^B p_{e,b}; q_b^R) \in \mathbb{R}^{n_h}$  while in the subsequent prediction steps only the pose of frame  $\{b\}$  and its first derivative are observed yielding  $u \in \mathbb{R}^{n_u}$ . Subsequently, the network is trained on data  $\mathcal{D} = \{\{y_{k,j}, u_{k,j}, h_j\}_{k=1}^{n_r}\}_{j=1}^{n_b}$  where the indice  $k$  denotes a time step, the indice  $j$  a trajectory, and  $y = ({}^B p_{e,B}; {}^B \dot{p}_{e,B})$  denotes the state of frame  $\{e\}$ . We refer to  $x_{k+1} = f(h, u_k)$  as an one step ahead prediction and to the sequence  $(h_k; f(h_k, u_k); f(f(h_k, u_k)); \dots)$  as a rollout.

*Our goal is to learn a model  $f$  to predict  $y_{k+1} = f(h, u_k)$  given the current observations  $h$  and  $u_k$  while also obtaining an approximation of the DLO's shape  $x_{k+1}$  from  $\mathcal{D}$ .*

To accomplish this goal, we develop the finite element inspired (FEI) network which consists of four essential components: i) an encoder mapping  $h(t_k)$  to  $x_k := x(t_k)$ , ii) a dynamics network predicting  $x_{k+1}$  from  $x_k$  and  $u_k$ , iii) a decoder mapping  $x_k$  and  ${}^B p_{b,B}(t_k)$  to  $y_k$ , and iv) a loss function that regularizes  $x$  during training. Summarizing, the contributions of this work are:

- i) We propose a novel data-driven DLO forward dynamics model that learns to predict the motion of a DLO from partial observations.
- ii) We demonstrate that forward kinematics of a body chain effectively enforces a human interpretable latent network state if used as a decoder.
- iii) We show that FEI networks generate physically plausible predictions of the DLO's shape by adding physics-inspired regularization terms into the regression problem.
- iv) We employ our proposed architecture to augment common data-driven dynamics models such as ResNet, RNNs, and NeuralODEs. In a robot experiment, we demonstrate that our model yields physically interpretability while marginally reducing prediction accuracy.

### 1.2 Related Work

The literature on DLO dynamics models can be classified based on the knowledge utilized for model synthesis, which includes employing first principles from physics, or system-specific data. While we structure the related work along these lines, the main contribution of our work revolves around describing and observing the DLO's latent state using forward kinematics arising from a rigid-FEM

discretization [11]. In turn, special emphasis is placed on the type of observations that are used by the different DLO dynamics models.

**Analytical physics-based models** Numerous works explore physics-based dynamics modeling of DLOs [12, 10, 13]. The interested reader is referred to [14] and the references therein for an in-depth discussion of the mechanics underlying DLO. The dynamics of DLOs can be conceptualized as an aggregation of infinitesimally small mass particles that interact through forces. To render the complicated particle interactions tractable for computational analysis, the finite element method (FEM) discretizes the continuous distribution of particles into finite elements. The R-FEM assumes that all particles inside an element form a rigid body such that their distances to each other remain fixed [11]. The R-FEM’s approximation results in a simplified representation of the DLO’s dynamics, but its accuracy lies at the mercy of the chosen force function and model parameters. While many commendable analytical models for these components exist, analytical models do often not suffice if we resort to small element counts or model DLOs with heterogeneous material properties. As R-FEM lies at the heart of our work, we discuss it in more detail in Section 2.

Other commonly found DLO dynamics models use finite differences approximations [14, 15] or piecewise constant curvature (PCC) models [16] which arise from a simplification of the Cosserat rod model [17, 6]. PCC models describe all points of the DLO using only a few curvature variables, thus avoiding the need for segmenting the body into discrete entities. Stella et al. used PCC to model the dynamics of a 2D underwater tentacle [18] and the kinematics of a 3D soft-continuum robot [19]. The effective integration of PCC models and Cosserat theory with NNs remains an unresolved challenge in current research, despite their promising potential in the field of DLO dynamics modeling.

**Data-driven models** Table 1 provides a summary of related data-driven DLO dynamics models. Our research is inspired by [20], who employed a long short-term memory (LSTM) [24] network to capture the input-output dynamics of a robot-arm-held pool noodle. In this study, the authors utilize the LSTM to predict the DLO’s endpoint positions from the pitch and yaw angles of the DLO’s start being held by the robot arm. For model predictive control (MPC) of the pool-noodles end, the authors use an extended Kalman filter (EKF) to estimate the latent states of the LSTM from observations. However, the EKF’s linearization of the DLO’s dynamics spawns approximation errors that limit control performance. In addition, the LSTM’s latent state lacks a physically meaningful representation, raising the question of how to incorporate physics principles to improve the model’s data efficiency while also hindering the formulation of physically meaningful constraints on the DLO’s latent state.

In related works, [21, 22] employed camera-based techniques to estimate the DLO’s center-line as a sequence of points. In [22], the dynamics of each point are predicted by an LSTM that shares with the other LSTMs its output history. Similarly, [21] introduced echo state networks (ESNs), where the output of an RNN serves as the input for a second RNN, in addition to control inputs and bending sensor measurements. In [5], DLO dynamics were modeled as a bi-directional LSTM (bi-

Table 1: Overview of related literature on data-driven modeling of DLO dynamics. While numerous works focus on the dynamics identification and observe the DLO’s full state through cameras, [20] and our work learns the dynamics by solely observing frames attached to the DLO’s start and end.

	System	Dynamics model	State type	Observer	Observer type
[18]	Submerged tentacle (2D)	PCC	Spline approx.	Full state	Computer vision
[21]	Submerged tentacle (2D)	ESN	Points	Full state	Computer vision
[22]	DLO in magnetic field	LSTMs	Points	Full state	Computer vision
[5]	Rope moved by robot arm	bi-LSTM	Particles	Full state	CNN
[23]	DLO attached to robot arm	bi-LSTM + GNN	Particles	Full state	IPS
[20]	DLO attached to robot arm	LSTM	Points	DLO ends	IPS + EKF
<b>Ours</b>	DLO attached to robot arm	e.g., <i>RNN, ResNet</i>	Rigid bodies	DLO ends	IPS + FK

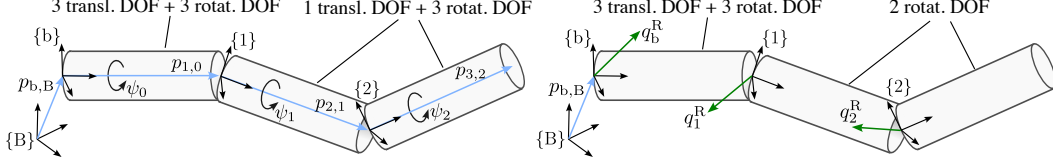


Figure 2: Generalized coordinate representations for a body chain. Left: The chain’s state is described through the distance vectors  $p_{i+1,i}$  and torsion variables  $\psi_i \in \mathbb{R}$ . Right: A more restrictive coordinate description uses a rotation description  $q_i^R$  in each joint.

LSTM) whose state is estimated from camera images using a CNN. Unlike previous works that used LSTMs to propagate states in time, the bi-LSTM propagates information along both directions of the DLO’s spatial dimension. Inspired by [5], [23] combined bi-LSTMs with graph neural networks (GNNs) [25]. In particular, [23] discretizes the DLO into a sequence of cylindrical elements similar to Cosserat theory [6] while the spatial and temporal element interactions are modeled through the NNs. However, these seminal works require cameras to obtain an estimation of several points on the DLO. The proposed FEI network potentially allows extending these methods to operate on partial observations while also enabling the incorporation of physics principles that stem from the extensive literature on multi-body dynamics.

## 2 A rigid FEM Perspective on data-driven DLO Dynamics

In what follows, we resort to R-FEM and model a DLO as a chain of  $n$  rigid bodies.

### 2.1 Kinematics of a DLO

As illustrated in Figure 2, the pose of the  $i$ -th body in the chain is described via a body-fixed coordinate frame  $\{i\}$ . The pose of  $\{e\}$  wrt. to  $\{B\}$  is described by the homogeneous transformation matrix

$${}^B T_e = \begin{bmatrix} {}^B R_e & {}^B p_{e,B} \\ 0 & 1 \end{bmatrix} \in \text{SE}(3) \quad (1)$$

with the position vector  ${}^B p_{e,B} \in \mathbb{R}^3$ , orientation matrix  ${}^B R_e \in \text{SO}(3)$ , and  $\text{SE}(3)$  denoting the special Euclidean group. In a chain of  $n$  bodies the pose of  $\{e\}$  wrt.  $\{B\}$  is obtained as

$${}^B T_e = {}^B T_b(q_b) \cdot {}^b T_1(q_1) \cdot {}^1 T_2(q_2) \cdots \cdots {}^{n-2} T_{n-1}(q_{n-1}) \cdot {}^{n-1} T_e, \quad (2)$$

where  $q_i$  denotes the generalized coordinates of the  $i$ -th joint,  $q_b = [{}^B p_{b,B}, {}^B q_b^R]$  denotes floating-base six degrees of freedoms (DOF) joint connecting  $\{b\}$  to  $\{B\}$  such that  ${}^B R_b = {}^B R_b({}^B q_b^R)$ . For modeling the relative motion of bodies in the serial chain, we use 2D revolute joints as depicted in Figure 2. While translatory DOFs are described through the entries of translation vectors, various coordinate descriptions exist for describing rotations. Typically used rotation descriptions  $q_i^R \subset q_i$  are Euler angles, quaternions, exponential coordinates [26], and position-twist angle pairs [27].

**Joint Types** While the spatial discretization of a DLO into segments is straightforward to understand, the question arises of how this perspective relates to the state representations used in prior works. As shown in Table 1, works on data-driven DLO dynamics modeling typically observe position vectors  ${}^B p_i$  along the DLO’s center line. As pointed out by [27] and used in [23], one can collect  $n + 1$  position vectors  ${}^B p_i$  along the DLO and interpret these as endpoints of  $n$  body segments. As illustrated in Figure 2, one then obtains  $n$  vectors  ${}^B p_{i+1,i} = {}^B p_{i+1} - {}^B p_i$  pointing from  ${}^B p_i$  to its successor  ${}^B p_{i+1}$  which denote two rotational DOFs of a body-fixed frame with origin at  $\{i\}$  and one translational DOF of a body-fixed frame with origin at  $\{i + 1\}$ . Surprisingly, the vector  $q = [{}^B p_0, {}^B p_{1,0}, {}^B p_{2,1}, \dots, {}^B p_{n-1,n-2}]$  is an almost complete coordinate description of a body chain having  $5 + 3(n - 1)$  DOF. The only DOF of a body chain that is not observed is the body torsion which can be added as  $n$  variables to  $q$  but requires additional observations. Note that this state description only pertains to R-FEM, if we either assume that the bodies are point masses as done in

[5, 23], or their lengths remain approximately constant. In summary,  $n + 1$  position vectors located along the DLO's center line describe almost the full pose (excluding torsion) of  $n$  segments that lie in between these points. In turn, learning to propagate this state description in time may be analyzed through the lens of R-FEM.

**Differential Kinematics** The goal of the FEI network is to predict the DLO's endpoint  ${}^B p_{e,B}$  and its velocity  ${}^B \dot{p}_{e,B}$  using only quantities that are observed during prediction time, namely the pose of frame  $\{b\}$  wrt.  $\{B\} - q_b = [{}^B p_{b,B}; {}^B \Psi_b] \in \mathbb{R}^6$ , its velocity  $\dot{q}_b$ , and its acceleration  $\ddot{q}_b$ . The DLO's endpoint position is obtained as

$${}^B p_{e,B} = {}^B p_{b,B} + {}^B R_b ({}^B q_b) {}^b p_{e,b}(q_1, \dots, q_{n_{el}}) = \text{fk}(q_b, q) \quad (3)$$

As detailed in [28, p. 111], differential kinematics describes the relation between  $\dot{q}$  and  ${}^B \dot{p}_e$  via the joint Jacobian matrix  $J_{\text{lin}}(q)$  as

$${}^B \dot{p}_{e,b} = J_{\text{lin}}(q) \dot{q} = \sum_{i=1}^{n_{el}} \frac{\partial {}^B p_{e,b}}{\partial q_i} \dot{q}_i. \quad (4)$$

## 2.2 Dynamics of a Rigid Body Chain

Designing an FEI network requires making informed decisions regarding the quantities that should be observed and fed into the model. We can draw inspiration from multibody dynamics to understand the causal structure needed for propagating the state of the DLO over time. For a rigid body chain, the Newton-Euler equation equates forces and torques acting on bodies and inside joints through inertia parameters via the equation of motion  $M(q)\ddot{q} = C(q, \dot{q}) + \tau(q, \dot{q})$ , with the generalized inertia matrix  $M(q) \in \mathbb{R}^{n_q \times n_q}$ , the bias force  $C(q, \dot{q}) \in \mathbb{R}^{n_q}$  and the joint torques  $\tau(q, \dot{q})$  [29, 26]. The formulation of the dynamics depends on what quantities we observe and which quantities we aim to predict. This gives rise to different types of dynamics formulations, namely forward dynamics, inverse dynamics, or hybrid dynamics. In the case of forward dynamics, the joint torques are known inputs, and the output of the model is the joint acceleration. Conversely, inverse dynamics involves predicting the joint torques based on the given joint acceleration.

When dealing with a DLO manipulated by a robot arm, the dynamics are governed by hybrid dynamics. That is, for the first body attached to  $\{b\}$ , the acceleration  $\ddot{q}_b$  is provided, while the corresponding joint torque  $\tau_b$  remains unobserved. For the subsequent bodies in the chain, our objective is to predict the accelerations  $\ddot{q}_i$  as a function of the joint torques  $\tau_i(q_i, \dot{q}_i)$ . An efficient implementation of hybrid dynamics is detailed in [30]. This algorithm provides valuable insight into the input-output structure of the hybrid dynamics of a rigid body chain. In particular, the hybrid dynamics algorithm given in [30] is a function of the form

$$\ddot{q} = f_{\text{HD}}(q_b, \dot{q}_b, \ddot{q}_b, q, \dot{q}, \theta_p), \quad (5)$$

where we used that the spatial velocity (aka twist) of the first body is obtained as  $T_{B,b}^{-1}(q_b) \dot{T}_{B,b}(q_b, \dot{q}_b)$ , that the joint torques  $\tau_i(q_i, \dot{q}_i)$  are assumed to be a function of the DLO's state, that the mechanical parameters  $\theta_p$  (e.g., element length, mass, and inertia) are constants, and that no external forces act on the DLO. A prediction of the next state is obtained by rewriting (5) in state-space form  $\dot{x} = f(x, u, \theta_p)$  and numerically integrating the current state via

$$x_{k+1} = \text{ODESolve}(f, x_k, u_k, \Delta t), \text{ with } \Delta t = t_{k+1} - t_k. \quad (6)$$

## 3 Finite Element Inspired Networks

The core idea driving the FEI network is to approximate a DLO as a serial chain of rigid bodies connected via elastic joints. Leveraging the FK of this chain as a decoder, we enforce a NN that models the dynamics of a DLO to learn the interactions between these bodies. This approach not only grants physical interpretability to the model but also enables the learning of DLO dynamics

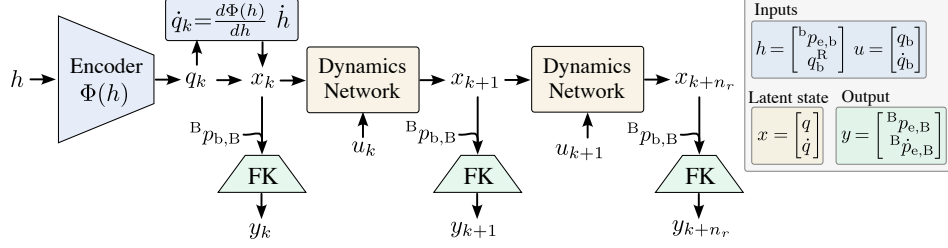


Figure 3: Architecture of an FEI network. By resorting to the FK of a serial chain and taking inspiration from R-FEM to determine the model’s inputs, the NN learns an encoding from partial observations to a physically-plausible latent state that is unrolled through time.

from partial observations, facilitates the reconstruction of the DLO’s shape, and paves the way for new avenues in physics-informed machine learning of DLO dynamics.

**Decoder** The decoder and encoder in the FEI network are inspired by the kinematics description of a serial chain of rigid bodies. The decoder equals the FK as given by (3) and (4). By using such a decoder, we ensure the interpretability of a NN that models the DLO’s dynamics, while maintaining a physically meaningful relationship between the latent states. To derive an FK decoder, we need to specify the type of joint between two bodies, provide the overall length of the DLO  $l_{\text{DLO}}$ , and select the number of elements  $n_{\text{el}}$  forming the body chain. Subsequently, using the uniform discretization method of the R-FEM [11], we obtain the length of the individual segment  $l_i$ . While the predictions of encoder and dynamics network do not require  ${}^B p_{b,B}$ , the FK requires  ${}^B p_{b,B}$  to obtain  $y$  from  $x$ .

**Encoder** The encoder, a feed-forward NN, predicts  $q = \Phi(h)$  from observations  $h$ , which corresponds to learning the inverse kinematics (IK) of a serial chain. The input  $h = ({}^B p_{e,b}; q_b^R)$  is invariant to the frame’s position in space as this information may diminish the network’s ability to generalize. The velocity variables  $\dot{q}$  are obtained by differentiating through the encoder as

$$\dot{q} = \frac{d\Phi}{dh}(h)\dot{h}, \quad (7)$$

which is straightforward to implement with automatic differentiation libraries such as JAX [31]. Note that (7) ensures that the velocity  $\dot{q}$  is the time derivative of  $q$  which would not be the case if we simply let an MLP predict  $\dot{q}$ .

If  $\dim(q) > \dim(h)$ , learning IK from observations becomes an ill-posed problem [32]. After all, multiple chain configurations can achieve the same end frame pose. While joint training of IK and dynamics may regularize  $q$ , we noticed that the encoder does not acquire a physically plausible state representation in its efforts to assist the dynamics network. Therefore, we introduce a regularization term in the loss to constrain the chain’s shape.

**Dynamics Network** The dynamics network unrolls the latent state  $x$  over time. This network occupies the same roll as the analytical hybrid dynamics as in (5) and (6). Under the assumption that R-FEM is a suitable for modeling a DLO, these equations inform us that the only additional vector required for unrolling  $x$  in time is  $u = (q_b; \dot{q}_b; \ddot{q}_b)$ .

**Loss Regularization** An FEI network is trained to minimize the loss function

$$\mathcal{L}_{\text{FEI}} = \frac{1}{n_b n_r} \sum_{j=1}^{n_b} \sum_{k=1}^{n_r} w_k \|y_{k,j} - \hat{y}_{k,j}\|_{W_y}^2 + \underbrace{\alpha_q q_{k,j}^\top q_{k,j}}_{\mathcal{L}_P} + \underbrace{\alpha_{\dot{q}} \dot{q}_{k,j}^\top \dot{q}_{k,j}}_{\mathcal{L}_K}, \quad (8)$$

with the model’s predictions  $\hat{y}_{k,j}$ , the weighting matrix  $W_y \in \mathbb{R}^{6 \times 6}$ , the state weight  $w_k$ , and regularization parameters  $\alpha_q$  and  $\alpha_{\dot{q}}$ . While the latter two terms in (8) can be simply seen as L2 regularization of the latent state  $x$ , we can look at these terms through the lens of R-FEM. In this regard, the  $\mathcal{L}_P$  in (8) minimizes a potential energy of linear spring forces acting between the elements while the  $\mathcal{L}_K$  minimizes the chain’s kinetic energy. While the kinetic energy of the body chain depends on the inertia matrix  $M(q)$ , it is lower and upper bounded by positive real constants



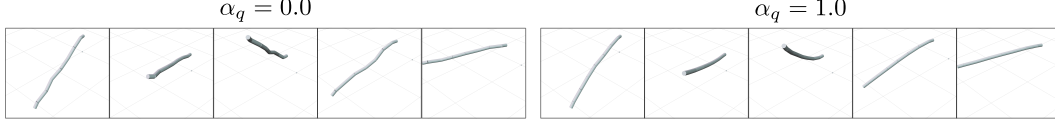


Figure 4: DLO shape predicted by a FEI network’s encoder with  $n_{el} = 7$ .

$\kappa_1 \leq M(q) \leq \kappa_2$  [28]. Accurate shape reconstruction from latent states potentially enables safe manipulation of DLOs in environments with obstacles. In the FEI networks, we can reconstruct the DLO’s shape from the encoder’s output predicting the state of the body chain. As illustrated in Figure 4, the chain’s shape notably depends on  $\alpha_q$ .

## 4 Results

To analyze the performance of different FEI networks, we aim to predict the motion of a 1.92 m long and 0.04 m thick aluminum rod that is rigidly connected to a Franka Panda robot arm. Two marker frames are attached to the DLO’s start and end. A “Vicon” camera-based IPS records the motion of these frames as depicted in Fig. 1. Before data collection, we performed a calibration routine to ensure that the transformations from the robot’s frame to the IPS’s world frame are accurate. During data collection, we recorded the Panda’s joint states, as well as several marker frame states with the Vicon system. During the data processing stage, we computed the inputs  $h_j$  and  $u_{k,j}$  and observations  $y_{k,j}$  using the calibrated kinematics and forward kinematics of the robot arm.

We collected nineteen trajectories from the robot amounting to 36 thousand data points. During the first half of a trajectory the robot arm moved the DLO; during the second half, the robot arm rested while the DLO kept moving. From sixteen trajectories, we used 15 % of the data for validation and the rest for training. For training and validation, the trajectories were split into rollouts of length 250, corresponding to one second of motion. The remaining three trajectories were used for testing and divided into rollouts using a sliding window of length 250.

**Data-driven Dynamics Models** As dynamics network of the FEI network we used several common NN, namely RNN with Gated Recurrent Units, ResNets, and second-order neural ODEs (NODE) – and denote the resulting models as FEI-RNN, FEI-ResNet, and FEI-NODE, respectively. As a baseline, we combine the same models with fully connected MLPs acting as encoder and decoder denoting the resulting models as RNN, ResNet, and NODE. Note that the MLP encoder predicts the full state  $x$  without enforcing  $\dot{q} = dq/dt$ . The FEI models are trained using the loss function (8) while the baseline NNs use an L2 loss. All models were implemented in JAX [31] using the Equinox library [33]. The NODE uses an adaptive stepsize (Dormand-Prince) Runge-Kutta integrator.

**Prediction Accuracy** As depicted in Figure 5 (Left), all the discrete-time models yield stable predictions during rollouts that extend significantly beyond the training rollout length  $r = 1$  s. In comparison, the NODEs start to diverge when the rollout length exceeds  $5 \times$  the training rollout length. Table 2 shows the model’s RMSE of the prediction of  ${}^B p_{e,B}$  and  ${}^B \dot{p}_{e,B}$ . Our findings indicate that models incorporating NN encoders and decoders slightly outperform the FEI models in terms of

Table 2: Model RMSEs of  ${}^B p_{e,B}$  and  ${}^B \dot{p}_{e,B}$ .  $r=1$  s is the rollout length used during training.

Model	Position RMSE [cm]					Velocity RMSE [cm/s]				
	$r$	$2r$	$5r$	$10r$	$20r$	$r$	$2r$	$5r$	$10r$	$20r$
NODE	3.0	4.1	12.7	24.6	60.3	2.5	3.5	12.5	22.2	49.7
FEI-NODE	3.4	4.5	8.1	48.0	169.7	3.2	4.0	5.4	9.2	22.4
ResNet	3.1	4.0	5.8	6.9	7.3	2.7	3.5	5.7	6.7	7.1
FEI-ResNet	3.7	4.5	6.0	6.2	6.6	3.3	4.1	5.8	5.9	6.3
RNN	2.9	3.5	3.9	4.9	5.7	2.4	2.9	3.3	4.3	5.3
FEI-RNN	3.4	4.0	4.7	6.4	7.1	3.3	3.9	4.6	6.3	6.9

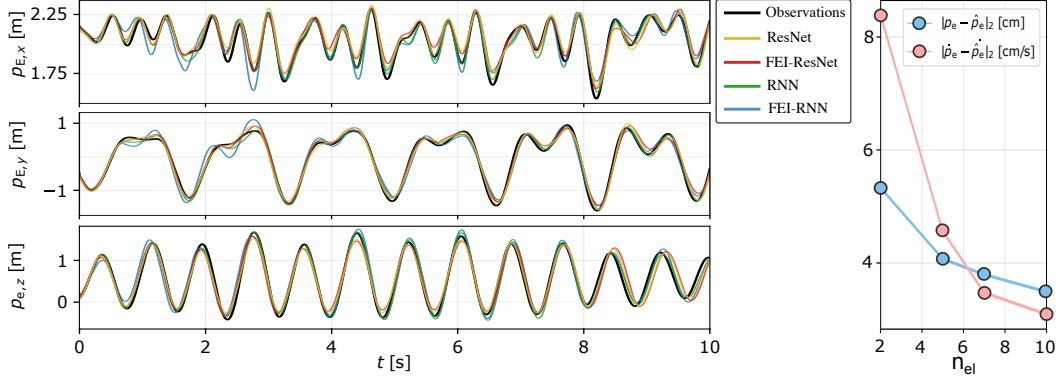


Figure 5: Left: Different model rollouts with the prediction time equaling 10 times the training rollout length  $r$ . Right: RMSE of a FEI-RNN over the number of elements  $n_{el}$ .

prediction accuracy. We posit that the FK decoder imposes constraints on the model which slightly reduces the model’s expressiveness. Notably, the NODE’s position error increases significantly faster than its velocity error which may potentially arise from the numerical integrator acting twice on the position error. Among models with a NN decoder, the RNN has a smaller RMSE than the ResNet after a rollout of  $20r$ . In comparison, the FEI networks’ RMSE at  $20r$  lies in between the RMSEs of the RNN and the ResNet. In terms of training time, NODE models are the slowest to train; one epoch of the NODE optimization takes almost as much time as 30 epochs of the RNN or ResNet models. The simulation time of all models are similar with the RNNs being the fastest ( $< 1$  ms), followed by the ResNets ( $\sim 4$  ms), and NODEs ( $\sim 5$  ms).

**Element Count** Figure 5 (Right) depicts the RMSE of the FEI-RNN model’s predictions on the test data. Initially, increasing the number of elements substantially reduces the error. This observation aligns with the common knowledge that discretization-based methods, like R-FEM, show improved model accuracy when increasing the number of elements. However, for R-FEM to model large DLO deformation it typically requires element counts going into the hundreds if not thousands which substantially increases the computational cost of R-FEM compared to an FEI network.

## 5 Conclusion

We have presented the first data-driven DLO dynamics model capable of accurately learning the motion of a DLO from partial observations while also acquiring a human interpretable latent state representation. Our model successfully predicted the position and velocity of a 1.92 m long aluminum rod, with its endpoint deviating up to 1.5 m from its equilibrium position, achieving in a twenty-second long simulation a sub-decimeter RMSE. This model was obtained by first deriving the FK of a rigid body chain approximating the DLO. At the first step of a rollout, the FK’s latent state is reconstructed from partial observations of the DLO’s start and end frames using an MLP encoder. In the subsequent time steps, the latent state is unrolled through time using a NN that effectively learns the system’s dynamics. All networks are trained jointly while we regularize the latent state to ensure that it acquires a physically plausible latent representation.

**Future Prospects and Limitations** We hope that the FEI network inspires the development of increasingly capable data-driven DLO dynamics model. In this regard, FEI networks may be seen as a framework whose components can be exchanged to improve prediction accuracy and incorporate additional desirable properties. While we used as dynamics NNs commonly encountered NNs, these models do not exploit the intricate spatial dependencies inherent in the DLO’s physics. In this regard, one could set up a FEI network using GNNs and/or Bi-LSTMs while connecting these works to articulated body algorithms as found in [30]. Alternatively, one could use as dynamics network models that respect energy conservation [34] or that respect implicit constraints [35]. While for the sake of illustration, we used Euler angles, future FEI networks may describe orientation using position-twist pairs [27] or Exponential coordinates [26]. As pointed out in [23], some coordinate



representations may prove advantages over others when learning dynamics. Moreover, while for the sake of illustration we parametrized the body chains using revolute joints, one may also use other joint types that better reflect certain physical properties of specific DLOs. Lastly, if future work extends the FEI networks to predict the full pose of  $\{e\}$  while being subject to external forces, then these models could be potentially used as practical building blocks in multibody simulators.

## References

- [1] J. Sanchez, J.-A. Corrales, B.-C. Bouzgarrou, and Y. Mezouar. Robotic manipulation and sensing of deformable objects in domestic and industrial applications: a survey. *The International Journal of Robotics Research*, 37(7):688–716, 2018.
- [2] P. Jiménez. Survey on model-based manipulation planning of deformable objects. *Robotics and computer-integrated manufacturing*, 28(2):154–163, 2012.
- [3] W. Wang, D. Berenson, and D. Balkcom. An online method for tight-tolerance insertion tasks for string and rope. In *2015 IEEE International Conference on Robotics and Automation (ICRA)*, pages 2488–2495. IEEE, 2015.
- [4] E. Yoshida, K. Ayusawa, I. G. Ramirez-Alpizar, K. Harada, C. Duriez, and A. Kheddar. Simulation-based optimal motion planning for deformable object. In *2015 IEEE international workshop on advanced robotics and its social impacts (ARSO)*, pages 1–6. IEEE, 2015.
- [5] M. Yan, Y. Zhu, N. Jin, and J. Bohg. Self-supervised learning of state estimation for manipulating deformable linear objects. *IEEE Robotics and Automation Letters*, 5(2):2372–2379, 2020.
- [6] D. K. Pai. Strands: Interactive simulation of thin solids using cosserat models. In *Computer graphics forum*, volume 21, pages 347–352. Wiley Online Library, 2002.
- [7] M. Saha and P. Isto. Manipulation planning for deformable linear objects. *IEEE Transactions on Robotics*, 23(6):1141–1150, 2007.
- [8] A. Karim and A. Verl. Challenges and obstacles in robot-machining. In *IEEE ISR 2013*, pages 1–4, 2013.
- [9] A. Verl, A. Valente, S. Melkote, C. Brecher, E. Ozturk, and L. T. Tunc. Robots in machining. *CIRP Annals*, 68(2):799–822, 2019. ISSN 0007-8506.
- [10] S. Drücker and R. Seifried. Application of stable inversion to flexible manipulators modeled by the absolute nodal coordinate formulation. *GAMM-Mitteilungen*, 46(1), 2023.
- [11] E. Wittbrodt, I. Adamiec-Wójcik, and S. Wojciech. *Dynamics of flexible multibody systems: rigid finite element method*. Springer Science & Business Media, 2007.
- [12] J. Spillmann and M. Teschner. Corde: Cosserat rod elements for the dynamic simulation of one-dimensional elastic objects. In *Proceedings of the 2007 ACM SIGGRAPH/Eurographics symposium on Computer animation*, pages 63–72, 2007.
- [13] J. Kim and N. S. Pollard. Fast simulation of skeleton-driven deformable body characters. *ACM Transactions on Graphics (TOG)*, 30(5):1–19, 2011.
- [14] M. Bergou, M. Wardetzky, S. Robinson, B. Audoly, and E. Grinspun. Discrete elastic rods. In *ACM SIGGRAPH 2008 papers*, pages 1–12. 2008.
- [15] H. Lang, J. Linn, and M. Arnold. Multi-body dynamics simulation of geometrically exact cosserat rods. *Multibody System Dynamics*, 25(3):285–312, 2011.
- [16] R. J. Webster III and B. A. Jones. Design and kinematic modeling of constant curvature continuum robots: A review. *The International Journal of Robotics Research*, 29(13):1661–1683, 2010.
- [17] J. Till, V. Aloï, and C. Rucker. Real-time dynamics of soft and continuum robots based on cosserat rod models. *The International Journal of Robotics Research*, 38(6):723–746, 2019.

- [18] F. Stella, N. Obayashi, C. D. Santina, and J. Hughes. An experimental validation of the polynomial curvature model: Identification and optimal control of a soft underwater tentacle. *IEEE Robotics and Automation Letters*, 7(4):11410–11417, 2022.
- [19] F. Stella, Q. Guan, J. Leng, C. Della Santina, and J. Hughes. Piecewise affine curvature model: a reduced-order model for soft robot-environment interaction beyond pcc. *arXiv preprint arXiv:2211.10188*, 2022.
- [20] J. A. Preiss, D. Millard, T. Yao, and G. S. Sukhatme. Tracking fast trajectories with a deformable object using a learned model. In *2022 International Conference on Robotics and Automation (ICRA)*, pages 1351–1357, 2022.
- [21] K. Tanaka, Y. Minami, Y. Tokudome, K. Inoue, Y. Kuniyoshi, and K. Nakajima. Continuum-body-pose estimation from partial sensor information using recurrent neural networks. *IEEE Robotics and Automation Letters*, 7(4):11244–11251, 2022.
- [22] A. Tariverdi, V. K. Venkiteswaran, M. Richter, O. J. Elle, J. Tørresen, K. Mathiassen, S. Misra, and Ø. G. Martinsen. A recurrent neural-network-based real-time dynamic model for soft continuum manipulators. *Frontiers in Robotics and AI*, 8:631303, 2021.
- [23] Y. Yang, J. A. Stork, and T. Stoyanov. Learning to propagate interaction effects for modeling deformable linear objects dynamics. In *2021 IEEE International Conference on Robotics and Automation (ICRA)*, pages 1950–1957. IEEE, 2021.
- [24] S. Hochreiter and J. Schmidhuber. Long short-term memory. *Neural computation*, 9(8):1735–1780, 1997.
- [25] F. Scarselli, M. Gori, A. C. Tsoi, M. Hagenbuchner, and G. Monfardini. The graph neural network model. *IEEE transactions on neural networks*, 20(1):61–80, 2008.
- [26] K. M. Lynch and F. C. Park. *Modern robotics*. Cambridge University Press, 2017.
- [27] B. Lefevre, F. Tayeb, L. Du Peloux, and J.-F. Caron. A 4-degree-of-freedom kirchhoff beam model for the modeling of bending–torsion couplings in active-bending structures. *International Journal of Space Structures*, 32(2):69–83, 2017.
- [28] B. Siciliano, L. Sciavicco, L. Villani, and G. Oriolo. Modelling, planning and control. *Advanced Textbooks in Control and Signal Processing*. Springer, 2009.
- [29] R. Featherstone. Rigid body dynamics algorithms. 2014.
- [30] J. Kim. Lie group formulation of articulated rigid body dynamics. Technical report, Technical report, Carnegie Mellon University, 2012.
- [31] J. Bradbury, R. Frostig, P. Hawkins, M. J. Johnson, C. Leary, D. Maclaurin, G. Necula, A. Paszke, J. VanderPlas, S. Wanderman-Milne, and Q. Zhang. JAX: composable transformations of Python+NumPy programs, 2018. URL <http://github.com/google/jax>.
- [32] M. I. Jordan. Constrained supervised learning. *Journal of Mathematical Psychology*, 36(3):396–425, 1992. ISSN 0022-2496.
- [33] P. Kidger and C. Garcia. Equinox: neural networks in JAX via callable PyTrees and filtered transformations. *Differentiable Programming workshop at Neural Information Processing Systems 2021*, 2021.
- [34] M. Lutter, C. Ritter, and J. Peters. Deep lagrangian networks: Using physics as model prior for deep learning. *arXiv preprint arXiv:1907.04490*, 2019.
- [35] A. Geist and S. Trimpe. Learning constrained dynamics with gauss’ principle adhering gaussian processes. In *Learning for Dynamics and Control*, pages 225–234. PMLR, 2020.